Integrated regulation of PKA by fast and slow neurotransmission in the nucleus accumbens controls plasticity and stress responses

Rachel Thomas[1,2], Adan Hernandez[2,3], David R. Benavides[2,4], Wei Li[5], Chunfeng Tan[2,6], Alan Umfress[7], Florian Plattner[2], Ayanabha Chakraborti[7], Lucas Pozzo-Miller[5], Susan S. Taylor[8], and James A. Bibb[2,5,7,]*

From the [1]Department of Neurology, University of Pennsylvania, Philadelphia, Pennsylvania, USA; [2]Department of Psychiatry, The University of Texas Southwestern Medical Center, Dallas, Texas, USA; [3]Departamento de Neurobiología Celular y Molecular, Instituto de Neurobiología, Universidad Nacional Autónoma de México, Juriquilla, Querétaro, México; [4]Department of Neurology, University of Maryland School of Medicine, Baltimore, Maryland, USA; [5]Department of Neurobiology, Civitan International Research Center, The University of Alabama Birmingham Medical Center, Birmingham, Alabama, USA; [6]Department of Neurology, McGovern Medical School, University of Texas Health Science Center at Houston, Houston, Texas, USA; [7]Department of Surgery, The University of Alabama Birmingham Medical Center, Birmingham, Alabama, USA; [8]Department of Chemistry and Biochemistry, University of California, San Diego, La Jolla, California, USA

Edited by Roger Colbran

Cortical glutamate and midbrain dopamine neurotransmission converge to mediate striatum-dependent behaviors, while maladaptations in striatal circuitry contribute to mental disorders. However, the crosstalk between glutamate and dopamine signaling has not been entirely elucidated. Here we uncover a molecular mechanism by which glutamatergic and dopaminergic signaling integrate to regulate cAMP-dependent protein kinase (PKA) *via* phosphorylation of the PKA regulatory subunit, RIIβ. Using a combination of biochemical, pharmacological, neurophysiological, and behavioral approaches, we find that glutamate-dependent reduction in cyclin-dependent kinase 5 (Cdk5)-dependent RIIβ phosphorylation alters the PKA holoenzyme autoinhibitory state to increase PKA signaling in response to dopamine. Furthermore, we show that disruption of RIIβ phosphorylation by Cdk5 enhances cortico-ventral striatal synaptic plasticity. In addition, we demonstrate that acute and chronic stress in rats inversely modulate RIIβ phosphorylation and ventral striatal infusion of a small interfering peptide that selectively targets RIIβ regulation by Cdk5 improves behavioral response to stress. We propose this new signaling mechanism integrating ventral striatal glutamate and dopamine neurotransmission is important to brain function, may contribute to neuropsychiatric conditions, and serves as a possible target for the development of novel therapeutics for stress-related disorders.

A fundamental function of brain circuitry is to impart emotional salience upon sensory input so that environmental experiences may be acted upon with appropriate behavioral responses. This requires the integration of fast ligand-gated ionotropic synaptic signals with those mediated by G-protein–coupled neurotransmitter receptors. Subserving these synaptic receptors, Ca^{2+} and cAMP are two principle second messengers that invoke overlapping intracellular signaling networks which compute the appropriate responses in the form of altered excitability and synaptic strength upon which learned behavioral responses are based. Understanding of the molecular mechanisms by which this is achieved is incomplete.

The nucleus accumbens (NAc, ventral striatum) is a central input structure within the basal ganglia and mediates reinforced learning and behavioral response processing. The medium spiny neurons (MSNs) in the NAc receive glutamatergic input from the medial prefrontal cortex, hippocampus, and other regions as well as dopaminergic input from the ventral tegmental area (1, 2). Coincidental detection of these two inputs is critical to reward, aversion, motor learning, and other aspects of sensory and emotional integration and behavioral flexibility (3, 4). The contributions of glutamate and dopamine to these critical brain functions are mediated by the interplay of key signaling pathways, such as the cAMP-dependent protein kinase (PKA) cascade (5–7).

The tetrameric PKA holoenzyme consists of two catalytic subunits (PKA_cat: Cα, Cβ, or Cγ isoforms) bound to a homodimer of regulatory subunits (RIα, RIβ, RIIα, or RIIβ isoforms). When RI subunits are incorporated, it is classified as Type I PKA, when bound to RII subunits as Type II PKA. R subunits possess an N-terminal dimerization domain (D/D), responsible for both dimerization and subcellular localization *via* binding to members of the A-kinase anchoring protein (AKAP) family of scaffolding molecules (8). Each R subunit monomer contains two C-terminal cyclic nucleotide-binding domains. Upon cAMP binding, PKA is activated by unleashing the catalytic activity from R dimer inhibition (9). Between the D/D and cyclic nucleotide-binding domains is a flexible linker region containing the inhibitor sequence (IS) responsible for occupying the C subunit active site in the inhibited state under basal conditions. The linker imparts an important structural

* For correspondence: James A. Bibb, jbibb@uab.edu.

distinction between Type I and Type II PKA, with functional implications for the holoenzyme. While the IS in Type I R subunits is a pseudosubstrate for PKA, the Type II IS acts as a true substrate for the C subunits at Ser95 on RIIα and Ser114 on RIIβ (10). Phosphorylation at the PKA site on RII subunits has been suggested to slow the reassociation rate of the R and C subunits (11, 12).

PKA activation engages many downstream effectors and signaling cascades, and many pathways impinge upon cAMP/ PKA signaling. The cAMP/PKA cascade may be activated by either ligand-gated ionotropic or G_s protein receptor-coupled metabotropic neurotransmission (6, 13). Previously, we showed that constitutive phosphorylation of DARPP-32 (14, 15) by cyclin-dependent kinase 5 (Cdk5) serves as an important mechanism by which glutamate and dopamine interact to regulate PKA signaling. Also, we reported that PKA-dependent activation of cAMP-specific phosphodiesterases is modulated though Cdk5-dependent phosphorylation of PDE4 family members (16). However, *direct* regulation of the PKA holoenzyme has not previously been shown to fall under the coordinated control of excitatory and metabotropic neurotransmission. We hypothesized that control of PKA activation/inhibition could serve as a critical point of integration for glutamate and dopamine inputs. Here we report a novel mechanism by which these two modes of neurotransmission are integrated to mediate ventral striatal circuitry function in plasticity and stress-response behavior.

Results

The PKA regulatory subunit RIIβ is a substrate for Cdk5

Messenger RNA transcripts encoding all four isoforms of the PKA regulatory subunit are present in brain, with expression of the RIIβ isoform enriched in the central nervous system (17–19). Examination of protein expression (Fig. 1A) indicates that the RIIβ subunit is most selectively expressed in brain compared to the other regulatory isoforms. Moreover, its brain region tissue distribution mimics the expression pattern of Cdk5. For both RIIβ and Cdk5, highest levels occur in limbic regions including prefrontal cortex, dorsal and ventral striatum, and hippocampus.

Immunostains of ventral striatum showed RIIβ in the soma and neuropil of MSNs where it colocalized with its scaffolding protein, AKAP150 (20, 21) (Fig. 1B). RIIβ colocalized with Cdk5 in dissociated rat striatal neurons grown in culture (Fig. 1C) and within cells and neuropil of rat striatal tissue. Furthermore, analysis of a rat NAc single nucleus RNA (snRNA-seq) library (22) revealed that RIIβ (*i.e.*, Prkar2b) and Cdk5 genes are co-expressed within subclusters of rat NAc cell populations including D1 and D2 dopamine expressing MSNs (D1-MSN, D2-MSN) and GABAergic and glutamatergic neurons (Fig. S1, A–E). Interestingly, RIIβ expression was absent from populations of astrocytic and oligodendritic cells (Fig. S1, B and D). Similarly, Cdk5 expression occurred in populations of D1-MSN, D2-MSN, GABAergic, and glutamatergic neurons and was also absent in astrocytic and oligodendritic cell

clusters (Fig. S1, C and E). Thus, Cdk5 and RIIβ are co-expressed within subcellular populations of the rat ventral striatum.

The amino acid sequence of RIIβ includes a proline-directed Cdk5 consensus motif (S/TPXK/H/R) within the N-terminal linker region predicting Thr69, a site unique to this particular R subunit, as a potential Cdk5 phosphorylation site. Indeed, Cdk5 phosphorylated pure recombinant RIIβ *in vitro*, achieving a maximal stoichiometry of 0.6 mol PO_4/mol of substrate under saturating conditions (Fig. 1, E and F). Mass spectrometry positively identified Thr69 as the site of phosphorylation, and the T69A site-directed mutant form of RIIβ was not phosphorylated by Cdk5 at all. To determine if this phosphorylation occurred in brain, a phosphorylation state-specific antibody for phospho-Thr69 RIIβ was derived (Fig. S1, F–H). Phospho-Thr69 RIIβ was detected within MSNs throughout the striatum by immunostaining (Fig. 1G). Together these data demonstrate that the RIIβ regulatory subunit of PKA is phosphorylated at Thr69 by Cdk5 and that this phosphorylation event occurs *in vivo* within striatal neurons.

Phosphorylation of RIIβ by Cdk5 affects PKA holoenzyme autophosphorylation kinetics

Both genetic deletion and pharmacologic inhibition of Cdk5 increases phosphorylation of PKA substrates in striatum (16). Thus, we hypothesized that Cdk5-mediated phosphorylation of Thr69 RIIβ could have an inhibitory effect on PKA_{cat} activity. However, *in vitro* analysis indicated that Thr69 phosphorylation did not alter the inhibition of PKA catalytic activity by RIIβ (Fig. S1I). Furthermore, phospho-memetic T69D mutation had no effect on cAMP-dependent activation of PKA in the RIIβ/PKA holoenzyme complex (Fig. S1J). As an alternative, we considered that Cdk5-dependent phosphorylation of Thr69 RIIβ could alter structure/function aspects of the holoenzyme inhibitory state. As mentioned above, the RIIβ D/D forms a four-helix bundle that docks with AKAPs through hydrophobic interactions (23, 24) (Fig. 2A). The Cdk5 phosphorylation site on RIIβ is encompassed within the flexible linker region that occurs between the D/D and the cAMP binding domains. This site is proximal to the IS in Type II R subunits, which contains the PKA phosphorylation site Ser114 (Fig. 2B). Therefore, we assessed the effect of phospho-memetic T69D mutation on PKA-dependent phosphorylation of Ser114 RIIβ (Fig. 2C). Interestingly, T69D phospho-mimetic mutation attenuated the efficiency of Ser114 phosphorylation by PKA in comparison to WT RIIβ, significantly reducing the maximum velocity of the reaction under linear conditions. Thus, the phosphorylation state of RIIβ at Thr69 may govern PKA "autophosphorylation" at Ser114.

To determine if this functional relationship between Thr69 and Ser114 RIIβ phosphorylation occurs *ex vivo*, acute striatal brain slices were treated with the Cdk5 inhibitor, CP681301 (Fig. 2D). Cdk5 inhibition attenuated the phosphorylation of

phospho-Thr69, with corresponding increase in PKA-dependent phosphorylation of Ser114. Together, these data reveal a novel intramolecular mechanism by which RIIβ phosphorylation is reciprocally regulated at two proximal sites *in vitro* and *ex vivo*.

Mechanistic function and regulation of RIIβ/PKA in ventral striatum

PKA regulation *via* RII subunit autophosphorylation has not previously been examined as a neuronal signaling mechanism. This may be because phosphorylation of RII by PKA characterizes the inhibited state of type II PKA holoenzymes (10). However, early studies suggested that phosphorylation at the PKA site could slow RIIβ reassociation with PKA$_{cat}$ following holoenzyme dissociation (11).

Consistent with this mechanistic function, phospho-mimetic S114D mutation of RIIβ reduced the PKA inhibition potency over 4-fold (IC$_{50}$ = 1.5 ± 0.3 nM, WT; 6.1 ± 1.1, S114D) (Fig. 3*A*). Thus, the level of PKA-dependent phosphorylation of Ser114, which occurs with formation of the PKA/RIIβ holoenzyme inhibitory state, may be controlled by the phosphorylation state of Thr69 RIIβ and may determine PKA inhibition potency by RIIβ. Therefore, neuronal activity which regulates Thr69 levels could modulate the efficacy of activators of G protein–coupled receptors that invoke the cAMP/PKA signaling cascade.

To further assess this possibility, the regulation of phospho-Thr69 and Ser114 RIIβ was explored in striatal slices. Acute N-methyl-D-aspartate (NMDA) treatment (50 μM, 5 min) strongly reduced the phosphorylation state of Thr69 (Fig. 3*B*).
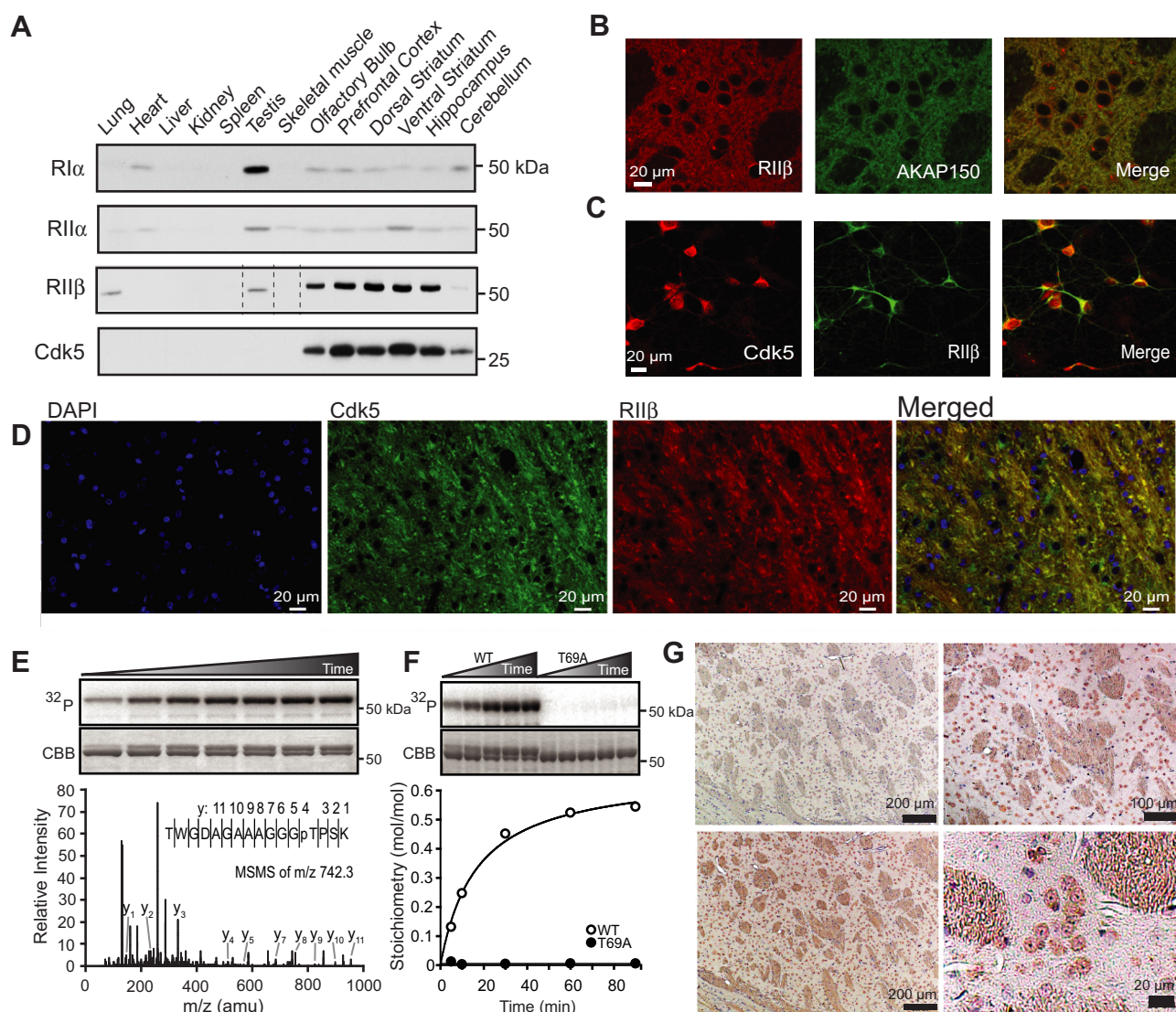

Figure 1. PKA regulatory subunit RIIβ phosphorylation at Thr69 by Cdk5. *A*, tissue distribution of R subunits and Cdk5 in rat peripheral and central nervous system tissues. For RIIβ blot, *dotted lines* denote the lane loaded for skeletal muscle was moved to correspond to the loading order for other blots. *B*, co-immunostain of RIIβ and AKAP150 in rat ventral striatum. *C*, colocalization of Cdk5 and RIIβ in dissociated rat striatal neurons. *D*, immunofluorescent colocalization of Cdk5 and RIIβ in rat striatum with nuclear DAPI counterstain. *E*, time-course *in vitro* phosphorylation of RIIβ by Cdk5 (autoradiogram, ^{32}P, *top*; Coomassie stain CBB, *middle*) with accompanying ESI-Qq TOF MS/MS spectrum (*bottom*) of the tryptic peptide shown encompassing phospho-Thr69 (pT, ion peak y4) positively identifying the site of RIIβ phosphorylation by Cdk5. *F*, *in vitro* phosphorylation of WT *versus* T69A RIIβ by Cdk5 with stoichiometry. *G*, immunostain of phospho-Thr69 RIIβ (*brown*, *top right*, and *bottom* two images) with nuclear counterstain (*purple*) in rat striatum. *Top left* image shows background with secondary antibody alone. AKAP, A-kinase anchoring protein; Cdk5, cyclin-dependent kinase 5; PKA, cAMP-dependent protein kinase.
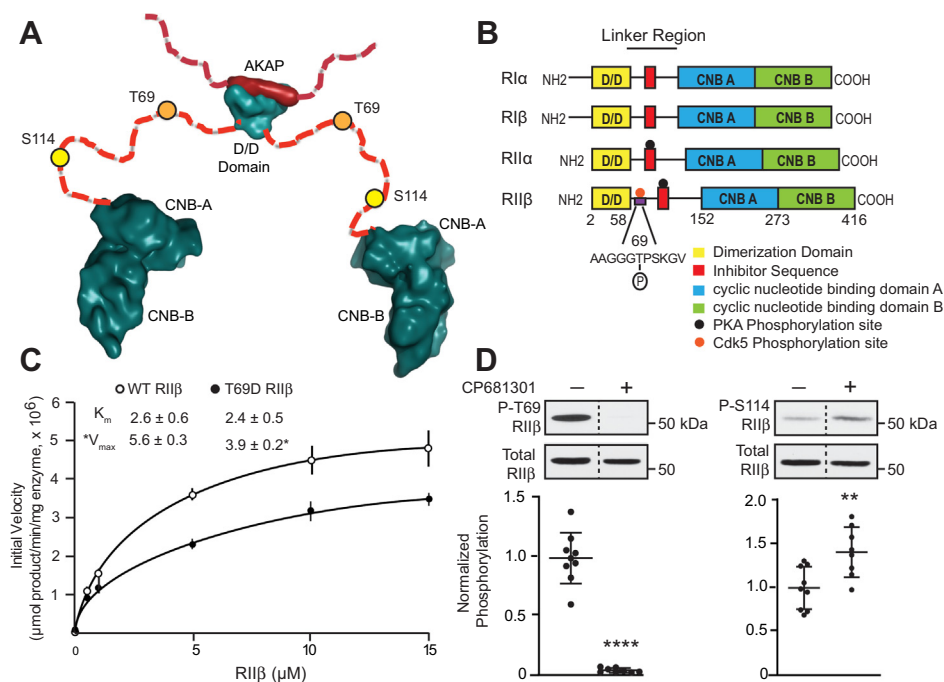
Figure 2. The phosphorylation state of Thr69 governs PKA-dependent phosphorylation of Ser114 RIIβ. *A*, structural model of RIIβ dimer complexed with AKAP showing the flexible linker region with Cdk5 and PKA sites denoted (24, 58). *B*, regulatory subunit isoforms of PKA with positions of structural/functional domains and phosphorylation sites indicated. *C*, kinetic analysis of *in vitro* autophosphorylation of Ser114 WT *versus* T69D RIIβ by PKA$_{cat}$ with K$_m$ and V$_{max}$ values. Data are means ± S.E.M., *$p < 0.05$, unpaired *t* test, n = 3. *D*, effects of striatal slice treatment with the Cdk5 inhibitor, CP681301 on phosphorylation of RIIβ at Thr69 (P-T69) by Cdk5 and Ser114 (P-S114) by PKA. Immunoblots of lysates from striatal slices treated with CP681301 (50 μM, 1 h) are shown with quantitation. *Dotted line* indicates where lanes were removed for example comparison. Data are normalized means ± S.D., ****$p < 0.0001$ for P-T69, **$p < 0.01$ for P-S114 RIIβ, unpaired *t* test, n = 8 to 9. AKAP, A-kinase anchoring protein; Cdk5, cyclin-dependent kinase 5; PKA, cAMP-dependent protein kinase.

Concomitantly, PKA-dependent phosphorylation at Ser114 was increased, consistent with the reciprocal modulation of these sites detected *in vitro* and in response to Cdk5 inhibition in intact brain tissue. The effect of NMDA on phospho-Thr69 appeared to be mediated by the activation of the Ca^{2+}-dependent serine/threonine protein phosphatase, PP2B (calcineurin), as the NMDA-induced reduction was blocked by the PP2B inhibitor cyclosporin A (Fig. S2A). Inhibition of protein phosphatases PP1 and PP2A by 1 μM okadaic acid also attenuated the effect of NMDA. Moreover, the basal phosphorylation state of phospho-Thr69 was increased by PP2B inhibition with cyclosporin A, PP1 inhibition by 1 μM okadaic acid, or selective PP2A inhibition with 200 nM okadaic acid (Fig. S2B). Together these data indicate that phospho-Thr69, and thereby phospho-Ser114, are regulated by activation of ionotropic NMDA class glutamate receptors. This is mediated, at least in part, through Ca^{2+}-dependent protein phosphatases including PP2B and 2A. These phosphatases together with PP1 also determine the basal phosphorylation state of phospho-Thr69 RIIβ. The diversity in protein phosphatases dephosphorylating RIIβ may not be surprising as both RII subunits interact with the serine/threonine phosphatase calcineurin (PP2B), Cdk5 complexes with PP2A (25), and AKAP signalosomes cluster protein phosphatases (26).

Phosphorylation at the Thr69 site modulates phosphorylation at Ser114, which in turn affects PKA inhibition by dissociated RIIβ. Therefore, NMDA-dependent modulation of Thr69 has the potential to impart effects upon PKA activation.

To test this, ventral striatal slices were treated with NMDA to activate fast neurotransmission, dopamine to activate slow neurotransmission, or both. As both NMDA and dopamine receptor activation are essential to the induction of striatal long-term potentiation (LTP) (27), these treatments were conducted under conditions similar to those used to induce striatal plasticity (Fig. 3C). Specifically, dopamine (10 μM) was bath-applied for 15 min with NMDA (25 μM) added for the last 5 min in reduced Mg^{2+} buffer with a 30 min delay following treatments. Effects on phospho-Thr69 RIIβ compared with PKA activity, as indicated by changes in PKA-dependent phosphorylation states of two key effectors, Ser845 GluA1 and Thr34 DARPP-32 (Fig. 3D). Under these conditions, NMDA again induced a decrease in phospho-Thr69 RIIβ, without significantly altering PKA activity. Dopamine alone also did not sustain PKA activity for 30 min. However, phospho-Thr69 reduction by combined dopamine and NMDA treatment corresponded to increased PKA activity 30 min after the treatments were removed (Fig. 3D). These data suggest a compound mechanism in which relatively high levels of phospho-Thr69 occur under basal conditions. Robust excitatory glutamatergic neurotransmission reduces phospho-Thr69 *via* protein phosphatase activation, resulting in increased PKA-dependent phosphorylation of Ser114 RIIβ. In the context of dopamine receptor activation, this leads to sustained elevated PKA activity involving downstream effector signaling pathways known to mediate synaptic plasticity and striatal function.
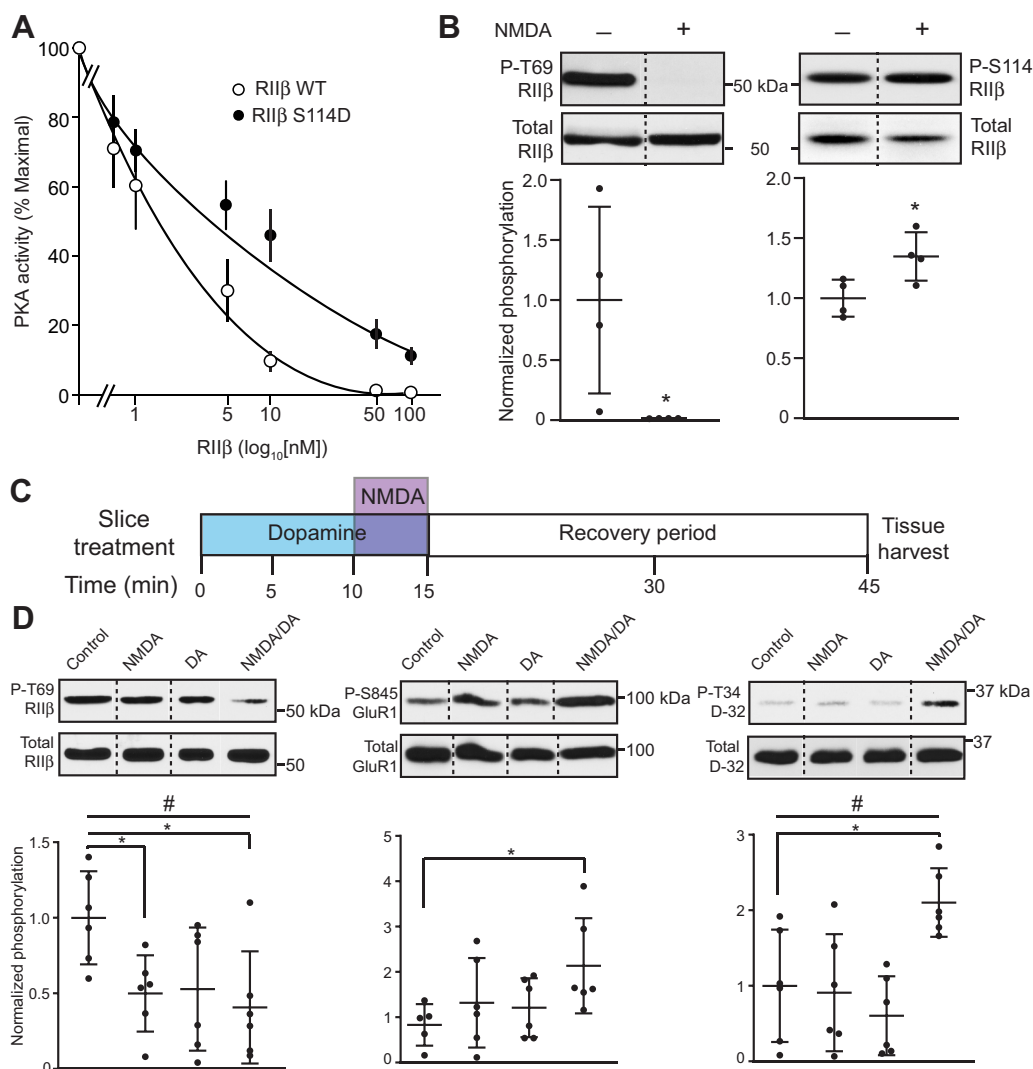
Figure 3. Reciprocal regulation of proximal RIIβ phosphorylation sites allow integration of glutamatergic and dopaminergic neurotransmission. *A*, PKA inhibition curves for WT *versus* S114D RIIβ. Data represent means ± S.E.M., IC_{50} = 6.1 ± 1.1 nM, S114D; 1.5 ± 0.3 nM, WT, n = 3. *B*, quantitative immunoblot analysis of lysates from striatal slices treated with NMDA (50 μM, 5 min) showing reciprocal regulation of the phospho-Thr69 and Ser114 RIIβ. *Dotted lines* denote where lanes were removed for exemplary blot comparisons. Data represent means ± S.D., *$p < 0.05$ for P-T69 and P-S114, unpaired *t* test, n = 4. *C*, schematic of NMDA/dopamine slice pharmacology cotreatment paradigm. *D*, effects of striatal slice treatment with NMDA (25 μM, 5 min), dopamine (DA, 10 μM, 15 min), or both on Cdk5-dependent phosphorylation of Thr69 RIIβ (*left*), and PKA-dependent phosphorylation of Ser845 GluR1 (*middle*) and Thr34 DARPP-32 (*right*). *Dotted lines* denote where lanes were removed for exemplary blot comparisons. Data represent means ± S.D. and were analyzed using the one-way ANOVA, $F_{(3,20)}$ = 3.67, #p = 0.029 for Thr69 RIIβ; $F_{(3,19)}$ = 2.42, p = 0.09 for Ser845 GluR1; $F_{(3,20)}$ = 6.29, #p = 0.003 for Thr34 DARPP32 followed by Newman-Keuls *post hoc*, *$p < 0.05$ compared to respective controls for Thr69 RIIβ and Thr34 DARPP-32 respectively. For Ser845 GluR1, *$p < 0.05$ (Control *versus* NMDA/DA), unpaired *t* test, n = 5 to 6. Cdk5, cyclin-dependent kinase 5; PKA, cAMP-dependent protein kinase.

RIIβ phosphorylation controls ventral striatal plasticity

To directly assess the contribution of the RIIβ regulatory phosphorylation mechanism to striatal function, a small interfering peptide (siP) was developed which corresponded to 18 amino acid residues from the RIIβ linker region encompassing Thr69 and included a membrane-permeabilizing penetratin tag (Fig. 4*A*, top). This Thr69 RIIβ siP (RIIβ siP) potently inhibited Cdk5-dependent phosphorylation of RIIβ (IC_{50} = 7.14 ± 2.28 μM) (Fig. S3*A*). Treatment of ventral striatal slices with this peptide caused reduction in phospho-Thr69 RIIβ but had no effect on Cdk5-dependent phosphorylation of Thr75 DARPP-32 (Fig. 4*A*, bottom). RIIβ siP/ dopamine cotreatment of ventral striatal slices resulted in a sustained increase in PKA activity, similar to the previously

observed effects of NMDA/dopamine treatment (Fig. S3*B*). Consequently, we established the means to selectively modulate phospho-Thr69 RIIβ levels in intact brain tissue and facilitate prolonged PKA activation.

With this reagent in hand, we chose to assess the role of RIIβ phosphorylation in cortico-ventral striatal plasticity as one measure of physiological function. Cortical afferents within corpus callosum of sagittal brain slices were stimulated, and field excitatory postsynaptic potentials (fEPSPs) were recorded in ventral striatum core (Fig. S4*A*). LTP was induced by high-frequency stimulation (HFS) and could be enhanced by 15 min bath application of the D1-type dopamine receptor agonist SKF81297 (Fig. S4*B*), as previously observed for dorsolateral striatum (27). To assess the contribution of RIIβ
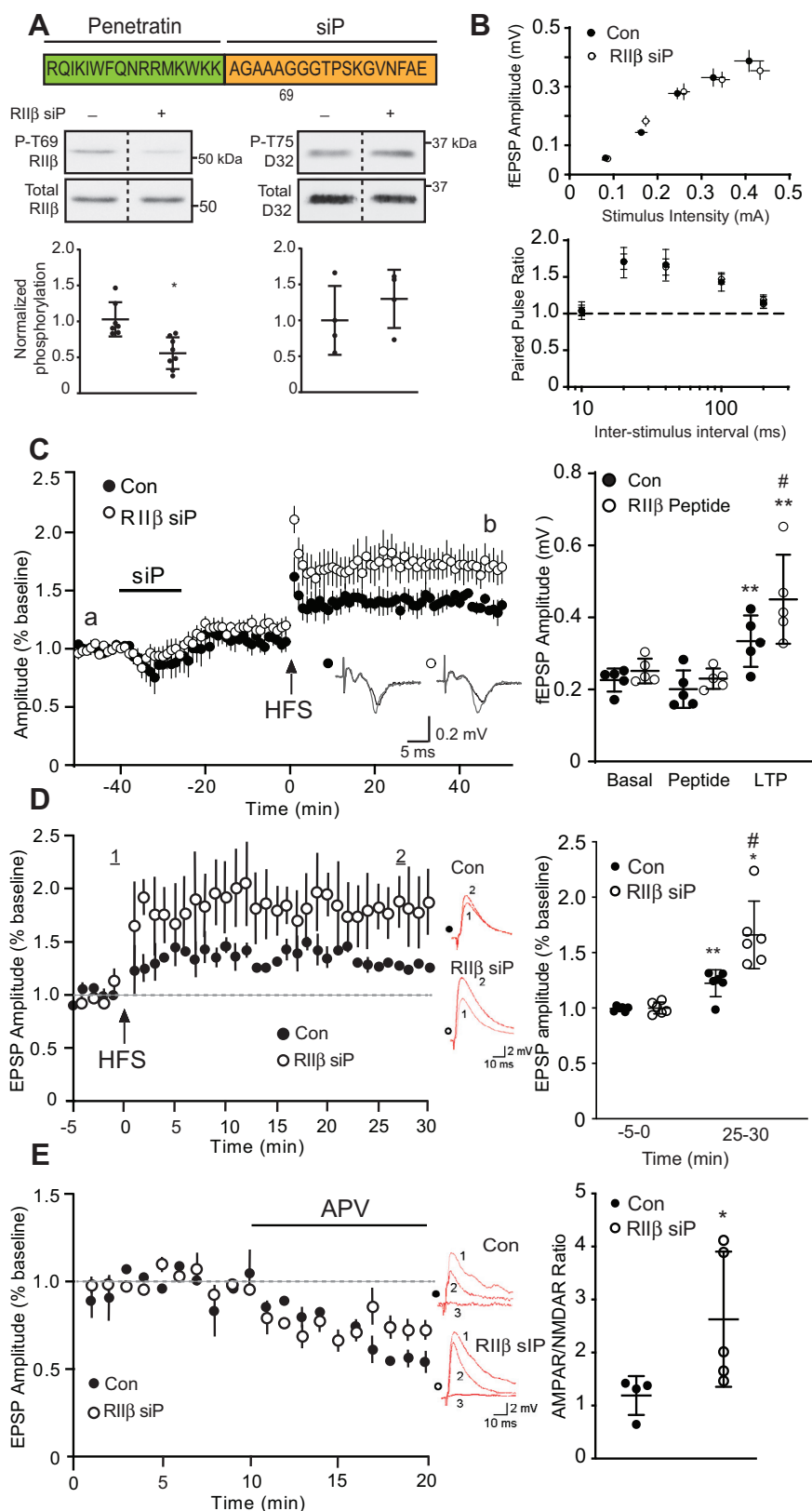
Figure 4. Selective interference of Thr69 RIIβ phosphorylation enhances ventral striatal plasticity. *A*, sequence of the RIIβ-targeting siP (*top*) and immunoblots of lysates from NAc slices treated with Th69 RIIβ siP (10 μM, 1 h). *Dotted lines* denote where lanes were removed for exemplary blot comparisons. Data represent means ± S.D., $*p < 0.05$, unpaired *t* test, n = 4 to 8. *B*, input/output (I/O) curves and paired pulse ratio (PPR) derived from cortico-ventral striatal fEPSP recordings of scrambled peptide control (Con) and RIIβ siP-treated slices. *C*, effects of RIIβ siP on NAc LTP assessed by field recordings. Plot of fEPSP amplitudes with sample traces from a *versus* b are shown (*left*) with summary plot (*right*) ($^{#}p < 0.05$ compared to scrambled peptide control, unpaired *t* test; $**p < 0.01$ compared to basal for RIIβ siP treated slices, Wilcoxon test, n = 5). *D*, effect of RIIβ siP on LTP in D1R neurons. EPSP amplitude following HFS of cortico-ventral striatal circuitry (*top*). Inset shows representative traces of EPSPs in current-clamp mode before and 25 min

phosphorylation to LTP, equilibrated slices were treated with either the RIIβ siP or a scrambled siP (control, 10 μM) for 15 min, followed by drug washout for 25 min prior to HFS (Fig. 4, B and C). The RIIβ siP had no effect on synaptic excitation (input-output, I/O) or paired pulse response ratios. RIIβ siP caused a transient reduction in basal fEPSP amplitude but significantly enhanced LTP compared to scrambled control siP, causing elevations in fEPSP amplitudes that were maintained through 50 min following HFS (0.31 ± 0.03 mV scrambled siP *versus* 0.45 ± 0.06 mV for RIIβ siP). Interestingly, the enhancement of LTP by the RIIβ siP was partly occluded in slices pretreated with SKF-81297 (2 μM) prior to HFS (Fig. S4, C and D).

To better understand this effect, whole cell patch-clamp recordings were made of D1R-expressing neurons (28). As observed in field recordings, the RIIβ siP induced a significant increase in EPSP amplitude and markedly elevated LTP levels in comparison to control treated neurons (Fig. 4D). This effect was attributable to increased α-amino-3-hydroxy-5-methyl-4-iso-xazolepropionic acid receptor (AMPAR)-mediated function, as AMPA/NMDA ratios were increased by the RIIβ siP (Fig. 4E), consistent with elevated phospho-Ser845 GluR1, which is linked to increased synaptic surface AMPAR trafficking (29) Thus, direct siP targeting of Thr69 RIIβ phosphorylation enhances cortico-ventral striatal plasticity, likely by increasing PKA activity. These findings together with the slice signaling data (see Fig. 3) are consistent with the modulation of RIIβ phosphorylation and PKA activity by NMDA and dopamine as an important mechanism mediating ventral striatal plasticity.

RIIβ regulation is altered by stress and can be targeted to affect stress-related behaviors

Synaptic plasticity and cognition are affected by stress (30–32). While acute stress can improve cognitive performance, exposure to persistent stress causes cognitive impairment (33, 34). To determine if stress could alter the signaling state of RIIβ phosphorylation, rats were exposed to a stressful environment either once (acute stress, one forced swim) or chronically (chronic unpredictable stress, two stressors daily for 14 days). Interestingly, 1 h following exposure to acute stress, phospho-Thr69 RIIβ was significantly decreased (Fig. 5A). In contrast, chronic exposure to stress caused elevation in the phosphorylation state of this site. Thus, environmental exposure to stressful conditions can alter the basal signaling state of RIIβ, raising the intriguing possibility that the regulation of RIIβ phosphorylation may contribute to behavioral responses induced by stress. Additionally, this mechanism may be targeted to modify behavioral responses to stress.

To examine this possibility, bilateral intra-accumbens infusions of the RIIβ siP *via* cannula were conducted. Delivery of

FITC-tagged RIIβ siP to ventral striatal core MSNs was confirmed by immunostains (Fig. 5B). RIIβ siP infusion induced increased PKA-dependent phosphorylation of Ser114 RIIβ, Ser845 GluA1, and Thr34 DARPP-32 *in vivo* (Fig. 5C), similar to its effects in slices. Incorporating this approach with behavioral studies, animals were subjected to the 2-day forced swim test (FST. Fig. 5D). On day 1, animals that had undergone intra-accumbal cannulation were made to swim for 8 min. The following day, subjects were infused with either the RIIβ siP or a scrambled control peptide, then re-exposed to the stress of forced swimming. RIIβ siP-infused subjects spent significantly less time immobile (Fig. 5E, left). The RIIβ siP effect was completely blocked by co-administration of the PKA inhibitor, PKI. No changes in immobility time were detected when PKI alone was infused. Moreover, none of these infusions had a significant effect on latency to immobility in the FST or locomotor activity (Fig. S5, A and B). Immobility was significantly less for animals that received the RIIβ siP during the 4 to 6 and 6 to 8 min periods of forced swimming compared to controls receiving scramble peptide (Fig. S5C). Also, the RIIβ siP's effects closely mimicked those of the rapid-acting antidepressant, ketamine, administered at subanesthetic levels *via* bilateral intra-accumbal infusion. These findings demonstrate that RIIβ phosphorylation in the NAc mediates behavioral reactions to a stressful environment and that these responses may be altered by pharmacological targeting of this integrative mechanism.

Together these findings support a signaling scheme (Fig. 5F) where the PKA/RIIβ holoenzyme can be shifted to a form where Thr69 RIIβ is less phosphorylated in response to excitatory glutamatergic neurotransmission and more phosphorylated at Ser114. In this state, upon activation of Gs-coupled D1 dopamine receptor signaling, PKA activation may be prolonged, thereby contributing to synaptic plasticity and behavioral responses. Thus, the equilibrium between different regulatory states of PKA may be an important determinant of behavioral responses to stress and overall mood.

Discussion

Emotional salience is imparted upon environmental experiences through integration of cortical glutamatergic and midbrain dopaminergic neurotransmission. The striatum integrates these inputs to mediate reward, motivation, and behavioral flexibility, allowing for learned behavioral responses to rewarding or aversive stimuli (35). The predominant second messengers that mediate dopaminergic and excitatory glutamatergic activity are cAMP and Ca^{2+}, respectively. These signaling modes can act antagonistically by activating protein phosphorylation or dephosphorylation of the same substrate

---

post-LTP induction. Summary data (*right*) show effect of RIIβ siP (10 μM, 1 h) *versus* control (scrambled siP). Data represent means ± S.D.; **$p < 0.01$ compared to control baseline, *$p < 0.05$, compared to RIIβ siP baseline, #$p < 0.05$, compared to LTP in controls, Student's *t* test, n = 4 to 6. E, effect of RIIβ siP on EPSP amplitude and response to selective ionotropic glutamate receptor antagonists in D1R neurons. Control and RIIβ siP-treated NAc slices underwent NMDAR antagonist APV (20 μM) treatments. Subsequent treatments with the AMPAR antagonist NBQX (10 μM) ablated EPSP responses (see inset). EPSP recordings (30 min after HFS, LTP induction) and APV effects are shown. Insets show traces for D1R neurons before (1) and after APV (2), and combined APV/NBQX (3) treatments. Summary data are presented (*right*) for AMPA/NMDA ratios. Data are means ± S.D., *$p < 0.05$, Student's *t* test n = 4 to 6. fEPSP, field excitatory postsynaptic potential; HFS, high-frequency stimulation; LTP, long-term potentiation; NAc, nucleus accumbens.
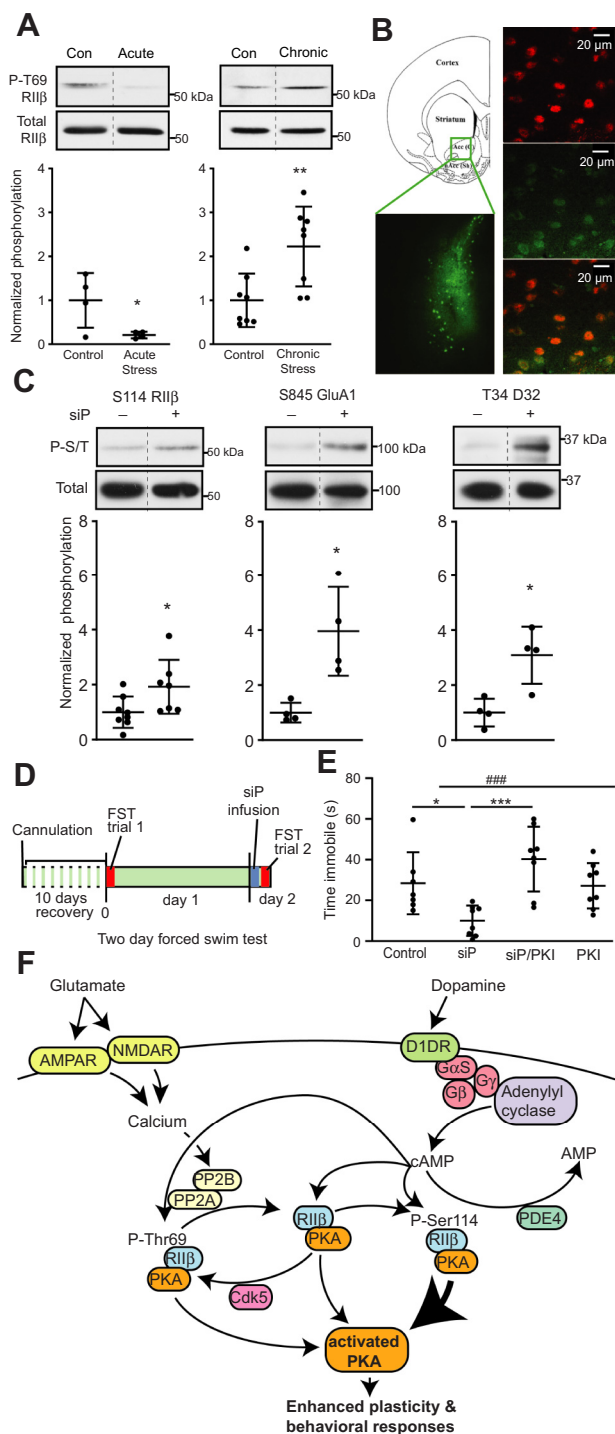
Figure 5. Intra-accumbens targeting of RIIβ regulation improves behavioral responses to stress. *A*, immunoblots of NAc lysate from animals exposed to acute *versus* chronic stress. *Dotted lines* denote where lanes were removed for exemplary blot comparisons. Data are means ± S.D., *p < 0.05, **p < 0.01, unpaired *t* test, n = 4 to 8. *B*, immunostain of FITC-labeled Thr69 RIIβ siP in nucleus accumbens core. Anatomical diagram shows region of injection and siP detection (*left*) with labeling of MSNs with nuclear NeuN (*red*) counterstain and siP (*green*) in soma and neuropil (*right*). *C*, immunoblots of lysates from ventral striatum taken 1 h after scrambled (−) *versus* RIIβ-siP (+) infusion. *Dotted lines* denote where lanes were removed for exemplary blot comparisons. Data are means ± S.D., *p < 0.05, unpaired *t* test, n = 4 to 7. *D*, depiction of experimental plan for peptide infusion and FST. *E*, FST analysis of effects of bilateral intra-accumbens infusions of control (scrambled peptide), RIIβ siP, and/or PKI. Data were analyzed using the one-way ANOVA (F(3,27) ###p = 0.0008 followed by

site. However, they may function most critically when working synergistically to invoke downstream effectors that alter neuronal excitability (36). For example, integration may occur upstream of PKA, at the level of cAMP metabolism, as both Ca^{2+}/CaM-dependent adenylyl cyclase (37, 38) and phosphodiesterases (39) can control cAMP/PKA signaling. cAMP/PKA and Ca^{2+} cascades can also converge at key effectors downstream of PKA such as DARPP-32 (40) and CREB (41). Here, we reveal convergence directly upon the RIIβ/PKA_{cat} holoenzyme complex as a fundamental mechanism of glutamate and dopamine integration.

The novel mechanism by which phosphorylation of the RIIβ regulatory subunit governs PKA holoenzyme activation involves the ability of Cdk5-dependent phosphorylation of Thr69 to reduce PKA autophosphorylation of Ser114 RIIβ. Phosphorylation at Ser114 has the net effect of increasing PKA activity by reducing the ability of RIIβ to inhibit PKA_{cat} once activated. Both Thr69 and Ser114 are located within the nonstructural linker region of RIIβ that occurs between the AKAP binding/D/D and cAMP-binding portion of RIIβ. Despite the high level of flexibility in this region, the linker has been demonstrated to play an important role in the overall conformation of the PKA holoenzyme. Holoenzymes containing RIIβ are the most structurally compact compared to those of other regulatory isoforms despite possessing the longest linker sequence of any R subunit (42). This feature is conferred by the unique sequence of the RIIβ linker region itself, as substitution of the RIIβ linker into RIIα renders holoenzyme structural density similar to that of PKA_{cat}/RIIβ (43). Phosphorylation of the proline-directed Thr69 site may also impart constraints or conformational changes in RIIβ secondary structure that prevent S114 from optimally occupying the catalytic pocket of PKA. Ongoing studies are aimed at solving the structural basis for these effects and better understanding how Ser114 phosphorylation attenuates PKA inhibition. Detailed understanding of the interactions between RIIβ, PKA_{cat}, and other protein kinases and phosphatases in the context of AKAP signalosomes (44) which contribute to synaptic plasticity (45) also remains an important area of investigation.

D1-dopamine receptor and glutamatergic NMDAR coactivation enhances striatal plasticity (5) and is required to achieve cortico-striatal LTP in dorsolateral striatum (27). PKA phosphorylation of DARPP-32 (46, 47) and GluA1 (48) both contribute to striatal plasticity. Phosphorylation of Thr34 facilitates plasticity by converting DARPP-32 into a potent PP1 inhibitor, thereby potentiating PKA activity. Phosphorylation at Ser845 GluA1 enhances AMPAR insertion into postsynaptic membranes, a necessary step in LTP. Here, modulation of RIIβ

phosphorylation either *via* NMDAR activation or with an RIIβ siP resulted in PKA-dependent phosphorylation of GluA1, DARPP-32, and likely other downstream effectors. Importantly, selective reduction of phospho-Thr69 RIIβ markedly improved cortico-striatal LTP in ventral striatum, consistent with the known functional contributions of these pathways.

Ventral striatal plasticity is thought to be crucial for coordination of behavioral responses to stressful environments through reinforcement learning and the encoding of rewarding *versus* aversive stimuli (49). Proper integration of fast and slow neurotransmission may be required for accurate assignment of emotional salience to stimuli and appropriate goal-directed behavioral responses, such as avoidance (50). Here, acute stress caused dephosphorylation of Thr69 RIIβ, and intra-accumbens reduction of Thr69 RIIβ increased struggle in response to re-exposure to forced swim stress. Thus, the regulation of RIIβ phosphorylation and its consequent effects on PKA activity may be an important mechanism mediating stress response behavior.

Chronic exposure to stress caused an increase in the phosphorylation state of Thr69 RIIβ. Acute stress can improve behavioral and mental acuity (51). However chronic and unpredicted stress can result in a range of deleterious effects including cognitive impairment (33) and is a major predisposing factor for mental illnesses such as major depressive disorder (52). Elevated levels of stress hormones have been linked to suppression of PKA signaling (53). Furthermore, dysregulation of the PKA pathway has been implicated in psychiatric disorders including depression (54). Thus, cAMP/PKA signaling presents an important target for drug therapy. Indeed, antidepressant medications often act either directly or indirectly upon G protein–coupled catecholamine receptors that modulate cAMP/PKA signaling. However, therapies that act at the receptor level often cause unwanted side effects. Thus, more direct manipulation of cAMP/PKA signaling is an attractive alternative approach to antidepressant treatment. Here we show that targeting of PKA signaling *via* an RIIβ siP to alter plasticity and behavioral function. It will be interesting to further explore the mediators of this effect including possible contributions from cFos and δFosB as well as less well-defined mechanisms. If RIIβ phosphorylation can be targeted by small compounds to achieve similar effects as those demonstrated here using the RIIβ siP, perhaps improved health care for mood disorders may be achieved.

Experimental procedures

Experimental model and subject details

Ten- to 14 week-old male Sprague-Dawley rats (Charles River, strain code 400) were used for most animal experiments and maintained on a 12 h light/dark cycle, single- or double-housed (chronic stress paradigm only) in standard cages, with food and water available *ad libitum* unless otherwise specified (*e.g.*, food restriction in chronic stress paradigm). For single unit patch clamp recordings, Drd2-EGFP mice in an FVB background were used. All manipulations were approved by UT Southwestern Medical Center and University of Alabama at Birmingham Institutional Animal Care and Use Committees and conducted in accordance with the NIH *Guide for the Care and Use of Laboratory Animals*.

Antibodies and reagents

All chemicals were purchased from Sigma-Aldrich unless otherwise specified. The sequence of the penetratin-tagged RII β-siP and penetratin-tagged scramble control peptides were RQIKIWFQNRRMKWKK-AGAAAGGGTPSKGVNF AEE and RQIKIWFQNRRMKWKK-AAGAGSGAVAFKGA NGEA or RQIKIWFQNRRMKWKK-AGAAAGGGAPR KGVNFAEE, respectively. The FITC-tagged siP was synthesized with an N-terminal FITC label.

Protein purification, in vitro phosphorylation, and phosphorylation site identification

Rat recombinant RIIβ was derived as a C-terminal 6XHis fusion by Ni-NTA affinity purification using standard pET vector methods (Novagen). RIIβ was phosphorylated *in vitro* by Cdk5 or PKA using standard conditions (55). Cdk5/p25 was from Millipore, and PKA was from NEB. 32P incorporation was quantitated by PhosphorImager analysis. All kinetic analyses were conducted under empirically defined linear conditions. PKA activity was measured by phosphorylation of recombinant inhibitor-1 (56) or DARPP-32 (14). For phosphorylation site identification, preparatively phosphorylated RIIβ was subjected to nano-liquid chromatography tandem mass spectrometry as previously described (57). Digests were redissolved in 0.1% trifluoracetic acid and loaded onto a Zip-Tip with C_{18} resin (Millipore) for purification. Analysis was conducted using nanoelectrospray-QSTAR Pulsar I quadrupole time-of-flight tandem mass spectrometry (MDS Proteomics). Structural model of AKAP/RIIβ dimer interaction was based on published data of AKAP (PDB: 2HWN) (24) and RIIβ (PDB: 1CX4) (58).

Histology

Immunostains were performed as previously described (59). Briefly, coronal, frozen sections (30 μ) were microwaved in antigen retrieval solution (BioGenex) at 95 °C for 10 min, and tissue was costained for AKAP150 (C-20, Santa Cruz Biotechnology Cat# sc-6445 RRID:AB_2225905; 1:200) and RIIβ (BD Biosciences Cat# 610626, RRID: AB_397958; 1:2000). For rat striatal immunofluorescent colocalization of Cdk5 and RIIβ, anti-Cdk5 (Rockland Cat.# 200-301-163) with goat anti-mouse Alexa488 and goat anti-rabbit Cy3 (Jackson Immuno) were used with DAPI (4′,6-diamidino-2-phenylindole) blue-fluorescent DNA counterstain (Millipore Sigma). For phospho-T69 RIIβ staining, paraffin-embedded rat brain cryosections (5 μ) were made. The 1° antibody was used at 1:200 dilution. A phospho-T69 RIIβ antibody was generated as previously described (60) using the RII peptide GGT*PSKGC (asterisk denotes phospho-Thr; 1:500 2°). For FITC-peptide verification, a cannulated rat was infused with 200 μM FITC-penetratin siP (1 μl over 10 min). After 1 h, brains were collected, placed into a matrix, cut adjacent to the cannula

tracts, fixed in O.C.T., and snap frozen. Cryosections (10 μ) were then stained for FITC (Abcam Cat# ab19224 RRID:AB_732395; 1:400) and counterstained with NeuN (Millipore Cat# ABN78 RRID:AB_10807945; 1:1000).

For staining of primary cultured neurons, embryonic striatal neurons (E18) from Long Evans rats (Charles River Labs) were cultured 14 to 21 days *in vitro* on 12-mm coverslips, fixed, immunostained for Cdk5 and RIIβ using the above indicated antibodies and imaged as previously described (61).

Rat NAc single cell library analysis

Using an open-source software of single-nucleus RNA sequencing data from the rat ventral striatum (Ratlus) (22) Cdk5 and RIIβ were searched and segmented for adult-male Sprague Dawley control condition rats. Uniform Manifold Approximation Projections were generated across all cell types previously assessed (22). Feature plots displaying genes of interest across all cell types were generated, and violin plots indicating gene expression across six cell classes were exported for comparative analysis.

Acute slice pharmacology and quantitative immunoblotting

Slice pharmacology was conducted as previously described (62). Briefly, striatum was microdissected from 350 μ coronal rat brain slices, equilibrated for 1 h, 30 °C in Kreb's buffer with 10 μg/ml adenosine deaminase (Roche). Pharmacological treatments included CP681301 (provided by Pfizer): 0 to 50 μM, 1 h; NMDA: 25 or 50 μM, 5 min; dopamine: 10 μM, 15 min; siP: 10 μM, 1 h; okadaic acid (Cell Signaling): 0.2 or 1 μM, 1 h; and cyclosporin A: 10 μM, 1 h. The NMDA/dopamine cotreatments (NMDA 25 μM, 5 min; DA 10 μM, 15 min) were designed to mimic conditions used to induce striatal LTP (27). Briefly, conditions included low Mg^{2+} (0.5 mM) and a 30 min tissue recovery in drug-free buffer prior to harvest. Tissue was snap-frozen on dry ice. Immunoblotting was as previously described (63) and analyzed using Image J software (NIH). Data from immunoblots with phosphorylation-specific antibodies were normalized to total protein. Antibodies used included those for PKA regulatory subunits (BD Biosciences Cat# 610626, RRID: AB_397958; BD Biosciences Cat# 610609 RRID:AB_397943; BD Biosciences Cat# 612242 RRID:AB_399565), phospho-S114 RIIβ (BD Biosciences Cat# 612550 RRID:AB_399845), and NMDAR1 (BD Biosciences Cat# 556308 RRID:AB_396353), phospho-S845 GluA1 (PhosphoSolutions Cat# p1160-845 RRID:AB_2492128) and phospho-T34 DARPP-32 (PhosphoSolutions Cat# p1025-34 RRID:AB_2492068), and total GluA1 (Millipore Cat# 05-855R RRID:AB_1587070). Total DARPP-32 antibody was from H. Hemmings (Weill Cornell Medical College).

Electrophysiology

Adult rats were anaesthetized by isoflurane (Piramal Healthcare), and brains were placed in ice-cold sucrose saline solution (4 °C) containing (in mM): 87 NaCl, 75 Sucrose, 2.5 KCl, 1.25 NaH_2PO_4, 7 $MgCl_2$, 0.5 $CaCl_2$, 25 $NaHCO_3$, and 10 glucose (pH 7.4; saturated with 95% CO_2, 5% O_2). Parasagittal vibratome slices (350 μ thick) containing prefrontal cortex and NAc core were transferred into saline solution containing 125 NaCl, 2.5 KCl, 1.25 NaH_2PO_4, 1.3 $MgCl_2$, 2 $CaCl_2$, 25 $NaHCO_3$, and 25 glucose (pH 7.4; saturated with 95% CO_2; 5% O_2) and maintained for 20 min at 30 °C, then transferred to room temperature (22–25 °C) and allowed 1 h recovery. Slices were transferred to perfusion chambers placed within an upright microscope stage and visualized by infrared differential interference microscopy and a CCD Super Low Luminance camera (KT&C, Co., Ltd). Slices were perfused continuously with oxygenated saline solution (2–3 ml/min).

Extracellular recordings: fEPSPs were obtained at 25 °C in the presence of the $GABA_A$ antagonist (SR95531, Gabazine, 2 μM) and were evoked by square current pulses (0.2 ms) at 0.033 Hz with a bipolar stimulation electrode (FHC) placed at the border of corpus callosum separated by ∼300 to 500 μ from the recording electrode. The perfusion saline solution was partially modified (in mM): 0.5 $MgCl_2$, 1 $CaCl_2$, 3.5 KCl. Results were obtained using a stimulus intensity to induce 60% of the maximal fEPSP amplitude taken from the I/O curve of each slice. The paired pulse ratio (PPR) paradigm was applied using different inter-stimulus intervals and PPR changes were measured as PPR = second fEPSP amplitude/first fEPSP amplitude. After recording stable baseline for at least 10 min, LTP was induced by HFS (4 trains, 100 Hz, 1 s duration, separated by 20 s). fEPSP amplitude was monitored for at least 50 min after HFS to evaluate LTP. All recordings were performed using a Multiclamp 700B amplifier and filtered at 4 kHz and digitized with a Digidata 1440 with pClamp 10 software for data acquisition (Axon, Molecular Devices, LLC). Recording pipette was filled with the same extracellular solution as the perfusion bath (2–4 MΩ resistance).

For whole-cell recordings, Drd2-EGFP FVB mice were deeply anesthetized and transcardially perfused with ice-cold cutting artificial cerebrospinal fluid containing (in mM): 87 NaCl, 2.5 KCl, 0.5 $CaCl_2$, 7 $MgCl_2$, 1.25 NaH_2PO_4, 25 $NaHCO_3$, 25 glucose, and 75 sucrose, bubbled with 95% O_2/5% CO_2. Parasagittal slices were cut transversely at 300 μm using a vibrating blade microtome (VT1200S, Leica Microsystems). Slices were transferred to normal saline solution containing (in mM): 119 NaCl, 2.5 KCl, 2.5 $CaCl_2$, 1.3 $MgCl_2$, 1.3 NaH2PO4, 26 $NaHCO_3$, and 20 glucose at 32 °C for 30 min and then allowed to recover for 1 h at room temperature before recordings. Individual slices were transferred to a submerged chamber mounted on a fixed-stage upright microscope (Zeiss Axioskop FS) and continuously perfused at 30 °C with normal saline solution containing (in μM): 0 $MgCl_2$, 50 picrotoxin, and 10 glycine. GFP-negative D1 cells were visualized by infrared differential interference contrast microscopy with a water-immersion 63X objective (0.9 NA, Zeiss). Current clamp recordings were performed with unpolished pipettes containing (in mM): 140 K-gluconate, 5 KCl, 2 $MgCl_2$, 10 Hepes, 4 Mg-ATP, 0.3 Na-GTP, 10 Na_2-creatine phosphate, 0.2 Na-EGTA, 290 to 300 mOsm, pH 7.3 (final resistance, 3-4MΩ). LTP of EPSPs was induced by HFS in control and RIIβ siP-treated D1 cells (at –70 mV). Slices were incubated in the presence of 10 μM control or RIIβ siP for 1 h and washed out

prior to recordings. Following LTP, slices were perfused with the NMDAR antagonist D-AP5 (20 µM) and the AMPAR antagonist NBQX (10 µM). All recordings were acquired with Axopatch-200B amplifiers (Molecular Devices), filtered at 2 kHz, and digitized at 10 kHz with ITC-18 A/D-D/A interfaces (InstruTech) controlled by custom-written software in G5 PowerMac computers (TI-WorkBench, provided by Dr Takafumi Inoue).

Stereotaxic surgeries

Rats were anesthetized with isoflurane and placed in a stereotaxic frame (Kopf Instruments). Bilateral cannulas (3 mm center-to-center distance, cut 8 mm below pedestal, Plastics One) were placed in NAc core (anterior-posterior to bregma +1.5 mm, medial/lateral ±1.5 mm, depth −6.8 mm). Peptides were bilaterally infused 1 week later in awake and mobile animals. Injection volume was 1 µl of peptide (100 µM in PBS, 10% DMSO, per cerebral hemisphere). Animals were allowed to recover for 1 h prior to behavioral testing. Accuracy was confirmed by infusion of methylene blue dye or direct visualization of cannula tracts postbehavioral testing.

Behavioral analysis

The Porsolt FST was conducted as described previously (64). Briefly, one-trial forced swim was used for acute stress. Nonsurgerized rats underwent an 8 min swim in an 8-gallon transparent water filled cylinder at 24 to 25 °C. Animals recovered in their home cages for 1 h prior to brain dissection. The NAc was then microdissected for immunoblotting. For two-trial FST, rats recovered from surgical cannulation procedures for 7 days prior to behavioral testing. On day 1, animals were placed in the testing room for 1 h to acclimate. They then underwent an 8 min preswim. Video recording was performed from the swimming tank side to observe front and hind limb motion. Awake and mobile animals were bilaterally infused 24 h later with scrambled peptide or siP and/or PKI (1 µl,100 µM), or ketamine (2 µg in 1 µl) at a rate of 0.1 µl/min. They were then placed in a locomotor chamber, and locomotor activity was monitored for 30 min in circular donut-shaped locomotor chambers in the dark with a computer-monitored infrared photobeam system (MED-PC, Med Associates). Locomotor counts were defined as sequential adjacent beam breaks. Locomotor testing was followed by a 30 min recovery in home cages and then 8 min test swims. The last 6 min of the test were scored for latency to immobility and time immobile, with immobility defined as the time animals spent completely motionless.

The chronic unpredictable stress paradigm was performed as adapted from Willner (65). Animals were pair-housed for 14 days prior to testing. Four pairs of control animals received only regular cage cleaning and handling, while the four pairs of test animals were exposed to two stressors per day, chosen pseudorandomly, for 14 days. Stressors included: Cage crowding (4/cage, 2 h), overnight isolation (1/cage, 12 h), overnight food deprivation (12 h), overnight water deprivation (12 h), cage placed at 4 °C (45 min), cage placed on orbital shaker (1 h), forced swimming (4 min), reverse lighting for dark cycle (12 h), lights off mid-cycle (3 h), tilted cage (45°, 12 h), and aversive odor exposure (cat urine, 12 h). Animals did not experience any stressor more than four times during the testing period, and at least 3 days were allowed between any one specific stressor. Brains were harvested 12 h after final stressor.

Statistical analysis

Data are reported as mean or normalized mean ± standard deviation, unless specified otherwise. Statistical analysis comparing two means was performed using the Student's *t* test. In addition, for some comparisons the Wilcoxon signed-rank test was used where indicated. In some cases, the means for more than one group were compared by ANOVA with the appropriate *post hoc* comparison as specified in the figure legends using GraphPad Prism 6.0 unless stated otherwise. Where specified, two categorical variables were compared using a two-way ANOVA. For all experiments, $*p < 0.05$, $**p < 0.01$, $***p < 0.001$, $****p < 0.0001$ were considered significant. No statistical methods were used to predetermine sample sizes, but sample sizes are similar to those generally employed in comparable studies. Statistical analysis was conducted with n ≥ 4 except for *in vitro* biochemistry (n = 3).

Data availability

Further information and requests for resources and reagents should be directed to and will be fulfilled by the lead contact, Dr James A. Bibb (jbibb@uab.edu).

necessarily represent the official views of the National Institutes of Health.

Conflict of interest—The authors declare there are no conflicts of interest with the contents of this article.

Dedications—This paper is dedicated to the memory of Paul Greengard.

Abbreviations—The abbreviations used are: AKAP, A-kinase anchoring protein; AMPAR, α-amino-3-hydroxy-5-methyl-4-isoxazolepropionic acid receptor; Cdk5, cyclin-dependent kinase 5; D/D, dimerization domain; fEPSP, field excitatory postsynaptic potential; FST, forced swim test; HFS, high-frequency stimulation; IS, inhibitor sequence; LTP, long-term potentiation; MSN, medium spiny neuron; NAc, nucleus accumbens; NMDA, N-methyl-D-aspartate; PKA, cAMP-dependent protein kinase; PPR, paired pulse ratio; siP, small interfering peptide.

References

1. Salgado, S., and Kaplitt, M. G. (2015) The nucleus accumbens: a comprehensive review. *Stereotact. Funct. Neurosurg.* **93**, 75–93
2. Xu, L., Nan, J., and Lan, Y. (2020) The nucleus accumbens: a common target in the comorbidity of depression and addiction. *Front. Neural Circuits* **14**, 37
3. Uddin, L. Q. (2021) Cognitive and behavioural flexibility: neural mechanisms and clinical considerations. *Nat. Rev. Neurosci.* **22**, 167–179
4. Miyazaki, M., Noda, Y., Mouri, A., Kobayashi, K., Mishina, M., Nabeshima, T., *et al.* (2013) Role of convergent activation of glutamatergic and dopaminergic systems in the nucleus accumbens in the development of methamphetamine psychosis and dependence. *Int. J. Neuropsychopharmacol.* **16**, 1341–1350
5. Yagishita, S., Hayashi-Takagi, A., Ellis-Davies, G. C., Urakubo, H., Ishii, S., and Kasai, H. (2014) A critical time window for dopamine actions on the structural plasticity of dendritic spines. *Science* **345**, 1616–1620
6. Greengard, P., Allen, P. B., and Nairn, A. C. (1999) Beyond the dopamine receptor: the DARPP-32/protein phosphatase-1 cascade. *Neuron* **23**, 435–447
7. Yapo, C., Nair, A. G., Hellgren Kotaleski, J., Vincent, P., and Castro, L. R. V. (2018) Switch-like PKA responses in the nucleus of striatal neurons. *J. Cell Sci.* **131**, jcs216556
8. Omar, M. H., and Scott, J. D. (2020) AKAP signaling islands: venues for precision pharmacology. *Trends Pharmacol. Sci.* **41**, 933–946
9. Taylor, S. S., Zhang, P., Steichen, J. M., Keshwani, M. M., and Kornev, A. P. (2013) PKA: lessons learned after twenty years. *Biochim. Biophys. Acta* **1834**, 1271–1278
10. Zhang, P., Smith-Nguyen, E. V., Keshwani, M. M., Deal, M. S., Kornev, A. P., and Taylor, S. S. (2012) Structure and allostery of the PKA RIIbeta tetrameric holoenzyme. *Science* **335**, 712–716
11. Rangel-Aldao, R., and Rosen, O. M. (1976) Dissociation and reassociation of the phosphorylated and nonphosphorylated forms of adenosine 3′:5′-monophosphate-dependent protein kinase from bovine cardiac muscle. *J. Biol. Chem.* **251**, 3375–3380
12. Isensee, J., Kaufholz, M., Knape, M. J., Hasenauer, J., Hammerich, H., Gonczarowska-Jorge, H., *et al.* (2018) PKA-RII subunit phosphorylation precedes activation by cAMP and regulates activity termination. *J. Cell Biol.* **217**, 2167–2184
13. Sassone-Corsi, P. (2012) The cyclic AMP pathway. *Cold Spring Harb. Perspect. Biol.* **4**, a011148
14. Bibb, J. A., Snyder, G. L., Nishi, A., Yan, Z., Meijer, L., Fienberg, A. A., *et al.* (1999) Phosphorylation of DARPP-32 by Cdk5 modulates dopamine signalling in neurons. *Nature* **402**, 669–671
15. Nishi, A., Bibb, J. A., Snyder, G. L., Higashi, H., Nairn, A. C., and Greengard, P. (2000) Amplification of dopaminergic signaling by a positive feedback loop. *Proc. Natl. Acad. Sci. U. S. A.* **97**, 12840–12845
16. Plattner, F., Hayashi, K., Hernandez, A., Benavides, D. R., Tassin, T. C., Tan, C., *et al.* (2015) The role of ventral striatal cAMP signaling in stress-induced behaviors. *Nat. Neurosci.* **18**, 1094–1100
17. Cadd, G., and McKnight, G. S. (1989) Distinct patterns of cAMP-dependent protein kinase gene expression in mouse brain. *Neuron* **3**, 71–79
18. Ventra, C., Porcellini, A., Feliciello, A., Gallo, A., Paolillo, M., Mele, E., *et al.* (1996) The differential response of protein kinase A to cyclic AMP in discrete brain areas correlates with the abundance of regulatory subunit II. *J. Neurochem.* **66**, 1752–1761
19. Ilouz, R., Bubis, J., Wu, J., Yim, Y. Y., Deal, M. S., Kornev, A. P., *et al.* (2012) Localization and quaternary structure of the PKA RIβ holoenzyme. *Proc. Natl. Acad. Sci. U. S. A.* **109**, 12443–12448
20. Carr, D. W., Stofko-Hahn, R. E., Fraser, I. D., Cone, R. D., and Scott, J. D. (1992) Localization of the cAMP-dependent protein kinase to the postsynaptic densities by A-kinase anchoring proteins. Characterization of AKAP 79. *J. Biol. Chem.* **267**, 16816–16823
21. Murphy, J. G., Sanderson, J. L., Gorski, J. A., Scott, J. D., Catterall, W. A., Sather, W. A., *et al.* (2014) AKAP-anchored PKA maintains neuronal L-type calcium channel activity and NFAT transcriptional signaling. *Cell Rep.* **7**, 1577–1588
22. Savell, K. E., Tuscher, J. J., Zipperly, M. E., Duke, C. G., Phillips, R. A., 3rd, Bauman, A. J., *et al.* (2020) A dopamine-induced gene expression signature regulates neuronal function and cocaine response. *Sci. Adv.* **6**, eaba4221
23. Esseltine, J. L., and Scott, J. D. (2013) AKAP signaling complexes: pointing towards the next generation of therapeutic targets? *Trends Pharmacol. Sci.* **34**, 648–655
24. Kinderman, F. S., Kim, C., von Daake, S., Ma, Y., Pham, B. Q., Spraggon, G., *et al.* (2006) A dynamic mechanism for AKAP binding to RII isoforms of cAMP-dependent protein kinase. *Mol. Cell* **24**, 397–408
25. Plattner, F., Angelo, M., and Giese, K. P. (2006) The roles of cyclin-dependent kinase 5 and glycogen synthase kinase 3 in tau hyperphosphorylation. *J. Biol. Chem.* **281**, 25457–25465
26. Wong, W., and Scott, J. D. (2004) AKAP signalling complexes: focal points in space and time. *Nat. Rev. Mol. Cell Biol.* **5**, 959–970
27. Hernandez, A., Tan, C., Mettlach, G., Pozo, K., Plattner, F., and Bibb, J. A. (2016) Cdk5 modulates long-term synaptic plasticity and motor learning in dorsolateral striatum. *Sci. Rep.* **6**, 29812
28. Ade, K. K., Wan, Y., Chen, M., Gloss, B., and Calakos, N. (2011) An improved BAC transgenic fluorescent reporter line for sensitive and specific identification of striatonigral medium spiny neurons. *Front. Syst. Neurosci.* **5**, 32
29. Henley, J. M., and Wilkinson, K. A. (2013) AMPA receptor trafficking and the mechanisms underlying synaptic plasticity and cognitive aging. *Dialogues Clin. Neurosci.* **15**, 11–27
30. Russo, S. J., and Nestler, E. J. (2013) The brain reward circuitry in mood disorders. *Nat. Rev. Neurosci.* **14**, 609–625
31. Dwivedi, Y., and Pandey, G. N. (2000) Adrenal glucocorticoids modulate [3H]cyclic AMP binding to protein kinase A (PKA), cyclic AMP-dependent PKA activity, and protein levels of selective regulatory and catalytic subunit isoforms of PKA in rat brain. *J. Pharmacol. Exp. Ther.* **294**, 103–116
32. Aceto, G., Colussi, C., Leone, L., Fusco, S., Rinaudo, M., Scala, F., *et al.* (2020) Chronic mild stress alters synaptic plasticity in the nucleus accumbens through GSK3β-dependent modulation of Kv4.2 channels. *Proc. Natl. Acad. Sci. U. S. A.* **117**, 8143–8153
33. Yuen, E. Y., Wei, J., Liu, W., Zhong, P., Li, X., and Yan, Z. (2012) Repeated stress causes cognitive impairment by suppressing glutamate receptor expression and function in prefrontal cortex. *Neuron* **73**, 962–977
34. Bellani, R., Luecken, L. J., and Conrad, C. D. (2006) Peripubertal anxiety profile can predict predisposition to spatial memory impairments following chronic stress. *Behav. Brain Res.* **166**, 263–270
35. Hurtubise, J. L., and Howland, J. G. (2017) Effects of stress on behavioral flexibility in rodents. *Neuroscience* **345**, 176–192
36. Vanhoose, A. M., Clements, J. M., and Winder, D. G. (2006) Novel blockade of protein kinase A-mediated phosphorylation of AMPA receptors. *J. Neurosci.* **26**, 1138–1145
37. Wong, S. T., Athos, J., Figueroa, X. A., Pineda, V. V., Schaefer, M. L., Chavkin, C. C., *et al.* (1999) Calcium-stimulated adenylyl cyclase activity

is critical for hippocampus-dependent long-term memory and late phase LTP. *Neuron* **23**, 787–798

38. Dunn, T. A., Storm, D. R., and Feller, M. B. (2009) Calcium-dependent increases in protein kinase-A activity in mouse retinal ganglion cells are mediated by multiple adenylate cyclases. *PLoS One* **4**, e7877

39. Krishnamurthy, S., Moorthy, B. S., Xin Xiang, L., Xin Shan, L., Bharatham, K., Tulsian, N. K., *et al*. (2014) Active site coupling in PDE:PKA complexes promotes resetting of mammalian cAMP signaling. *Biophys. J.* **107**, 1426–1440

40. Scheggi, S., De Montis, M. G., and Gambarana, C. (2018) DARPP-32 in the orchestration of responses to positive natural stimuli. *J. Neurochem.* **147**, 439–453

41. Steven, A., Friedrich, M., Jank, P., Heimer, N., Budczies, J., Denkert, C., *et al*. (2020) What turns CREB on? And off? And why does it matter? *Cell Mol. Life Sci.* **77**, 4049–4067

42. Lu, T. W., Aoto, P. C., Weng, J. H., Nielsen, C., Cash, J. N., Hall, J., *et al*. (2020) Structural analyses of the PKA RIIβ holoenzyme containing the oncogenic DnaJB1-PKAc fusion protein reveal protomer asymmetry and fusion-induced allosteric perturbations in fibrolamellar hepatocellular carcinoma. *PLoS Biol.* **18**, e3001018

43. Vigil, D., Blumenthal, D. K., Heller, W. T., Brown, S., Canaves, J. M., Taylor, S. S., *et al*. (2004) Conformational differences among solution structures of the type ialpha, IIalpha and IIbeta protein kinase A regulatory subunit homodimers: role of the linker regions. *J. Mol. Biol.* **337**, 1183–1194

44. Torres-Quesada, O., Mayrhofer, J. E., and Stefan, E. (2017) The many faces of compartmentalized PKA signalosomes. *Cell Signal.* **37**, 1–11

45. Sanderson, J. L., and Dell'Acqua, M. L. (2011) AKAP signaling complexes in regulation of excitatory synaptic plasticity. *Neuroscientist* **17**, 321–336

46. Calabresi, P., Gubellini, P., Centonze, D., Picconi, B., Bernardi, G., Chergui, K., *et al*. (2000) Dopamine and cAMP-regulated phosphoprotein 32 kDa controls both striatal long-term depression and long-term potentiation, opposing forms of synaptic plasticity. *J. Neurosci.* **20**, 8443–8451

47. Yger, M., and Girault, J. A. (2011) DARPP-32, jack of all trades… master of which? *Front. Behav. Neurosci.* **5**, 56

48. Oliveira, R. F., Kim, M., and Blackwell, K. T. (2012) Subcellular location of PKA controls striatal plasticity: Stochastic simulations in spiny dendrites. *PLoS Comput. Biol.* **8**, e1002383

49. Volman, S. F., Lammel, S., Margolis, E. B., Kim, Y., Richard, J. M., Roitman, M. F., *et al*. (2013) New insights into the specificity and plasticity of reward and aversion encoding in the mesolimbic system. *J. Neurosci.* **33**, 17569–17576

50. Cahill, E., Salery, M., Vanhoutte, P., and Caboche, J. (2014) Convergence of dopamine and glutamate signaling onto striatal ERK activation in response to drugs of abuse. *Front. Pharmacol.* **4**, 172

51. Yuen, E. Y., Liu, W., Karatsoreos, I. N., Ren, Y., Feng, J., McEwen, B. S., *et al*. (2011) Mechanisms for acute stress-induced enhancement of glutamatergic transmission and working memory. *Mol. Psych.* **16**, 156–170

52. Scarpa, J. R., Fatma, M., Loh, Y. E., Traore, S. R., Stefan, T., Chen, T. H., *et al*. (2020) Shared transcriptional signatures in major depressive disorder and mouse chronic stress models. *Biol. Psych.* **88**, 159–168

53. Keil, M. F., Briassoulis, G., Stratakis, C. A., and Wu, T. J. (2016) Protein kinase A and anxiety-related behaviors: a mini-review. *Front. Endocrinol. (Lausanne)* **7**, 83

54. Yuan, L. L., Wauson, E., and Duric, V. (2016) Kinase-mediated signaling cascades in mood disorders and antidepressant treatment. *J. Neurogenet.* **30**, 178–184

55. Bibb, J. A., Nishi, A., O'Callaghan, J. P., Ule, J., Lan, M., Snyder, G. L., *et al*. (2001) Phosphorylation of protein phosphatase inhibitor-1 by Cdk5. *J. Biol. Chem.* **276**, 14490–14497

56. Nguyen, C., Nishi, A., Kansy, J. W., Fernandez, J., Hayashi, K., Gillardon, F., *et al*. (2007) Regulation of protein phosphatase inhibitor-1 by cyclin-dependent kinase 5. *J. Biol. Chem.* **282**, 16511–16520

57. Tassin, T. C., Benavides, D. R., Plattner, F., Nishi, A., and Bibb, J. A. (2015) Regulation of ERK kinase by MEK1 kinase inhibition in the brain. *J. Biol. Chem.* **290**, 16319–16329

58. Diller, T. C., Madhusudan, Xuong, N. H., and Taylor, S. S. (2001) Molecular basis for regulatory subunit diversity in cAMP-dependent protein kinase: crystal structure of the type II beta regulatory subunit. *Structure* **9**, 73–82

59. Nishi, A., Kuroiwa, M., Miller, D. B., O'Callaghan, J. P., Bateup, H. S., Shuto, T., *et al*. (2008) Distinct roles of PDE4 and PDE10A in the regulation of cAMP/PKA signaling in the striatum. *J. Neurosci.* **28**, 10460–10471

60. Czernik, A. J., Mathers, J., and Mische, S. M. (1997) Phosphorylation state-specific antibodies. In: Hemmings, H. C, ed. *Regulatory Protein Modification: Techniques and Protocols (Neuromethods, 30)*, Humana Press Inc, Totowa, NJ: 219–250

61. Kansy, J. W., Daubner, S. C., Nishi, A., Sotogaku, N., Lloyd, M. D., Nguyen, C., *et al*. (2004) Identification of tyrosine hydroxylase as a physiological substrate for Cdk5. *J. Neurochem.* **91**, 374–384

62. Nishi, A., Snyder, G. L., and Greengard, P. (1997) Bidirectional regulation of DARPP-32 phosphorylation by dopamine. *J. Neurosci.* **17**, 8147–8155

63. Sahin, B., Shu, H., Fernandez, J., El-Armouche, A., Molkentin, J. D., Nairn, A. C., *et al*. (2006) Phosphorylation of protein phosphatase inhibitor-1 by protein kinase C. *J. Biol. Chem.* **281**, 24322–24335

64. Castagne, V., Moser, P., Roux, S., and Porsolt, R. D. (2011) Rodent models of depression: forced swim and tail suspension behavioral despair tests in rats and mice. *Curr. Protoc. Neurosci.* **Chapter** 8, Unit 8 10A

65. Willner, P. (1997) Validity, reliability and utility of the chronic mild stress model of depression: a 10-year review and evaluation. *Psychopharmacology (Berl)* **134**, 319–329